

Keeping Representation Similarity in Finetuning for Medical Image Analysis

Wenqiang Zu^{1,4*}, Shenghao Xie^{2*}, Hao Chen³, Yiming Liang^{1,4}, Lei Ma^{2,4†}

¹ Institute of Automation, Chinese Academy of Sciences

² Academy for Advanced Interdisciplinary Studies, National Biomedical Imaging Center, National Key Laboratory for Multimedia Information Processing, Peking University

³ School of Chemical Sciences, University of Chinese Academy of Sciences

⁴ Beijing Academy of Artificial Intelligence

zuwenqiang2022@ia.ac.cn, shenghaoxie@stu.pku.edu.cn, lei.ma@pku.edu.cn

Abstract

Foundation models pretrained on large-scale natural images have been widely used to adapt to medical image analysis through finetuning. This is largely attributed to pretrained representations capturing universal, robust, and generalizable features, which can be reutilized by downstream tasks. However, these representations are later found to gradually vanish during finetuning, accompanied by a degradation of foundation model’s original abilities, e.g., generalizability. In this paper, we argue that pretrained representations can be well preserved while still effectively adapting to downstream tasks. We study this by proposing a new finetuning method RepSim, which minimizes the distance between pretrained and finetuned representations via constraining learnable orthogonal manifold based on similarity invariance. Compared to standard finetuning methods, e.g., full finetuning, our method improves representation similarity by over 30% while maintaining competitive accuracy, and reduces sharpness by 42% across five medical image classification datasets. The code will be released.

1. Introduction

Foundation models [2, 4, 46] pretrained on large-scale natural images have been shown to not only achieve outstanding performance on in-domain downstream tasks, but also exhibit impressive zero-shot learning abilities on out-of-domain tasks. In some cross-domain few-shot tasks, e.g., medical image analysis [18, 33, 41, 50], data is insufficient for training an equally powerful foundation model from scratch due to factors like privacy concerns, rare dis-

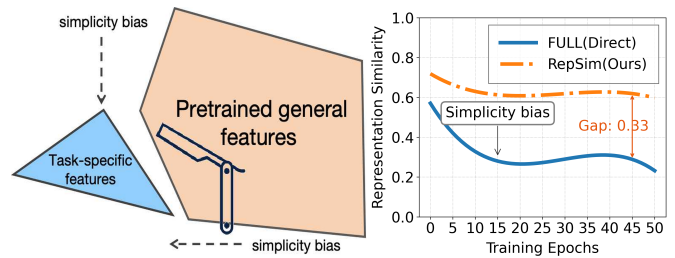


Figure 1. **Left:** Direct full finetuning just like the Occam’s Razor, tends to shave off merely task-specific features for the representation. RepSim (ours) is a better razor, additionally shaving off pretrained general features. **Right:** The simplicity bias occurs during full finetuning, whereas RepSim mitigates it effectively, maintaining a higher similarity with pretrained representations.

eases, and the high annotation cost [48]. As a result, finetuning [5, 16, 19, 31] has been proposed to adapt general foundation models to such tasks by training with a smaller learning rate, fewer epochs or parameters. In this way, finetuning is implicitly assumed to limit the Euclidean distance change of models in parameter space, thus ensuring effective adaptation to downstream tasks while preserving the foundation model’s original pretrained abilities, e.g., generalizability, which is beneficial for several scenarios, e.g., multi-task learning [44, 49] and continual learning [42].

However, recent works [24, 30, 35] find that the generalizability cannot be well preserved as expected, and impose additional constraints based on hyperspherical energy [28] to mitigate it (See detailed comparisons in Sec. 2.1). Inspired by the Occam’s razor in Minyoung *et al.* [17], i.e., simplicity bias hypothesis, we have another new intuition: The universal, robust, and generalizable features captured by pretrained representations are keys to achieve zero-shot generalization across most downstream tasks. However, for any individual

*Equal contribution.

†Corresponding author.

task among them, these general features may not be the most crucial for decision-making. As shown in Fig. 1 (Left), The representation tends to learn new, task-specific, and more discriminative features while ignoring general features during standard finetuning, even if they are compatible with the current task. To verify this, we introduce the representation similarity, measuring the distance between pretrained and finetuned representations based on CKA [23]. As shown in Fig. 1 (Right), it can be observed that similarity decreases during full finetuning. Later experiments also show that the performance on downstream tasks remains nearly unaffected after keeping a higher similarity. This leaves us wondering, *are pretrained representations destined to be used only once, like a flash in the pan?*

Let’s first consider one interesting phenomenon: There are extensive physical constraints in many biological systems, *e.g.*, protein molecules, leading to lower freedom degrees during evolution [11]. In systems with low freedom degree, functional sensitivity, *i.e.*, the system’s sensitivity to external perturbations, and mutational stability, *i.e.*, the system’s stability against internal perturbations, can be proven to be equivalent [39]. Inspired by this low-dimensionality dynamics, we find that finetuning also tends to constrain the freedom degree of foundation models due to its small parameter update range. During finetuning, similar to the functional sensitivity, the model is required to achieve high accuracy on current task as the input changes. Moreover, similar to mutational stability, as the parameter updates, the model is also required to maintain sufficient accuracy on other tasks. When the freedom degree of system is low, these two objectives do not conflict, allowing representations to retain the pretrained generalizability while also acquiring fitness to downstream tasks. Therefore, we can similarly introduce additional constraints, *i.e.*, representation similarity, to further reduce the model freedom degree and preserve pretrained representations.

A naive way to incorporate a similarity constraint is adding the hard regularization term [6] in loss function to directly minimize distance between pretrained and finetuned representations, but this incurs significant computational or storage overhead due to frequent similarity comparisons. To avoid this, we propose *RepSim* to make three efforts. First, we leverage the similarity property, *i.e.*, invariance to orthogonal transformation, to transform the problem into constraining finetuned representations within the orthogonal manifold of pretrained representations by learning only the orthogonal transformation matrix. Second, we compute the covariance of all representations for both pretraining and finetuning, and impose constraints based on these statistical information at once, rather than handling each representation individually. We also analyze representations at the last backbone layer to avoid layer-wise nonlinear activation function, which could disrupt the orthogonal manifold.

Our main contributions can be summarized below:

1. We demonstrate that pretrained representations with generalizability, can be well preserved during finetuning while still effectively adapting to downstream tasks.
2. We propose RepSim based on the representation similarity with a more efficient soft regularization.
3. Our method improves representation similarity by over 30% while maintaining competitive accuracy, and reduces sharpness by 42% across five medical image classification datasets compared to standard finetuning methods, *e.g.*, full finetuning, with superior effect to hard regularization, compatibility with other finetuning methods, *e.g.*, PEFT, and potential in multi-task learning.

2. Related Work

2.1. Finetuning

Typically, finetuning can be categorized into full finetuning [31] and parameter-efficient finetuning (PEFT) [8] methods. Full finetuning is retraining all parameters of the pretrained model [22, 26, 40]. PEFT trains only a subset of original or additionally introduced parameters, *e.g.*, prompt tuning [3, 19, 50], partial layer tuning [37, 47], adapter tuning [5, 14, 38], and LoRA [12, 16, 27].

In particular, orthogonal finetuning (OFT) [30, 35] has been proposed to preserve pretrained generation abilities. Although RepSim and OFT both leverage similar the orthogonal transformation invariance, differences exist in their derivation perspectives, *i.e.*, representation similarity *v.s.* hyperspherical energy [29]. Specifically, RepSim is a representation-based approach to minimize the distance between pretrained and finetuned representations, and achieves this by imposing manifold constraints on representation statistical information, *e.g.*, covariance. In contrast, OFT is a weight-based approach to remain rather than minimize the hyperspherical energy of pretrained models, and achieves this by constraining model weights. The solved problem is also different. OFT focuses on how to enhance performance of the finetuned task by preserving pretrained generation ability, whereas RepSim aims to preserve pretrained generalizability beneficial for other tasks without compromising performance on finetuned task. Thus RepSim also verifies the potential in common scenarios, *e.g.*, multi-task learning, beyond only validating its effectiveness on single tasks, *e.g.*, discrimination or generation.

2.2. Representation and Similarity

With the advancement of scaling laws [10, 20] and self-supervised learning [13, 34, 36], pretrained representations have captured rich and diverse features from real-world datasets, and are used to enhance the convergence of downstream tasks [15, 25, 43, 45]. Different similarity metrics have been proposed to compare representations across var-

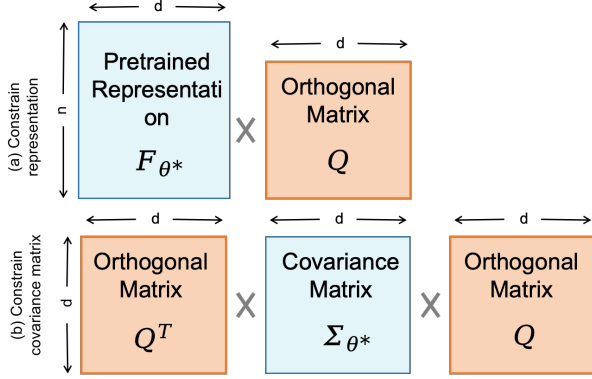


Figure 2. (a) Transform directly the pretrained representation matrix. (b) Transform orthogonally the covariance matrix.

ious layers or models to better understand neural network behaviors, e.g., CCA [32] and CKA [23], and these metrics exhibit various invariances, e.g., invertible linear transformation, orthogonal transformation, and isotropic scaling.

3. Method

Notations. Bold symbols denote matrices or vectors (e.g., \mathbf{X} and \mathbf{x}). Scalars are written in lowercase (e.g., x). For a matrix \mathbf{X} , \mathbf{X}_i (or equivalently, $\mathbf{X}_{i,\cdot}$) denotes its i th row. The dataset is given by $\mathcal{D} = \{(\mathbf{X}_i, y_i)\}_{i=1}^n$, where $\mathbf{X} \in \mathbb{R}^{n \times d}$ is the input samples for a model, n is the number of samples, and d is the dimension of features. The Frobenius norm is denoted by $\|\cdot\|_F$.

A model is represented by f_θ , where θ denotes the parameters; when omitted, we simply write f . The notation $\mathbf{F}_\theta(\mathbf{X})$ represents the features extracted by the model backbone, which is distinct from the classification output $f_\theta(\mathbf{X})$. The function $S(\cdot, \cdot)$ or $CKA(\cdot, \cdot)$ denotes a general similarity measure between two representations. For simplicity, we omit the dataset \mathbf{X} in $\mathbf{F}_\theta(\mathbf{X})$ and write it as \mathbf{F}_θ . We denote the pretrained (initial) parameters of the model as θ_0 .

3.1. Preliminary

Define the classification loss function:

$$\mathcal{L}_{\text{cls}}(\theta) = \mathbb{E}_{(\mathbf{X}, \mathbf{y}) \sim \mathcal{D}} \|f_\theta(\mathbf{X}) - \mathbf{y}\|^2 \quad (1)$$

where $\mathbf{y} = \{y_i\}_{i=1}^n$.

Definition 1 (Linear Centered Kernel Alignment). Let $\mathbf{F}_\theta \in \mathbb{R}^{n \times d}$ denote the feature matrix of input samples \mathbf{X} for model \mathbf{F}_θ with centered value:

$$\mathbf{F}_{\theta, \text{c}} := \mathbf{F}_\theta - \frac{1}{n} \mathbf{1} \mathbf{1}^\top \mathbf{F}_\theta \quad (2)$$

where $\mathbf{1} \in \mathbb{R}^n$ is the all-ones vector. The Linear Centered Kernel Alignment between two feature representations is

given by:

$$CKA(\mathbf{F}_{\theta_0}, \mathbf{F}_\theta) := \frac{\langle \mathbf{F}_{\theta_0, \text{c}} \mathbf{F}_{\theta_0, \text{c}}^\top, \mathbf{F}_{\theta, \text{c}} \mathbf{F}_{\theta, \text{c}}^\top \rangle_F}{\|\mathbf{F}_{\theta_0, \text{c}} \mathbf{F}_{\theta_0, \text{c}}^\top\|_F \|\mathbf{F}_{\theta, \text{c}} \mathbf{F}_{\theta, \text{c}}^\top\|_F} \quad (3)$$

The CKA metric fundamentally measures the alignment of covariance structures between feature representations. This alignment proves sensitive to dimensional collapse but remains invariant under orthogonal transformations and isotropic scaling, as formalized in the following invariance property.

Property 2 (Invariance Transformation). For any $\alpha > 0$ and orthogonal matrix $\mathbf{Q} \in O(d)$, the finetuned feature $\mathbf{F}_\theta = \alpha \mathbf{F}_{\theta_0} \mathbf{Q}$ satisfies:

$$CKA(\mathbf{F}_{\theta_0}, \mathbf{F}_\theta) = CKA(\mathbf{F}_{\theta_0}, \alpha \mathbf{F}_{\theta_0} \mathbf{Q}) = 1 \quad (4)$$

Definition 3 (Similarity-Invariant Subspace). For pretrained parameters θ_0 , define:

$$\mathcal{M}_{\theta_0} := \{\theta \in \Theta \mid \exists \mathbf{Q} \in O(d), \exists \alpha > 0 : \mathbf{F}_\theta = \alpha \mathbf{F}_{\theta_0} \mathbf{Q}\} \quad (5)$$

The invariant subspace \mathcal{M}_{θ_0} characterizes all representations that are equivalent to the pretrained model. Additional analysis is provided in the supplementary materials.

3.2. Problem Formulation

Given a pretrained model f_{θ_0} with parameters θ_0 , the objective is to obtain a finetuned model f_θ that simultaneously maximizes task-specific performance and maintains representation similarity. Formally, this constrained optimization problem can be formulated as:

$$\theta^* = \arg \min_{\theta} \mathcal{L}(\theta) \quad \text{subject to} \quad CKA(\mathbf{F}_{\theta_0}, \mathbf{F}_\theta) \geq \epsilon \quad (6)$$

Here $CKA(\cdot, \cdot)$ denotes the representation similarity metric with threshold $\epsilon \in [0, 1]$, and $\mathbf{F}_\theta \in \mathbb{R}^{n \times d}$ represents the feature representations extracted by the backbone of model f_θ .

Definition 4 (Hard-Constrained Similarity Loss: HCS). Let $\mathcal{L}_{\text{cls}}(\theta)$ denote the task-specific loss and $\mathcal{L}_{\text{sim}}(\theta)$ denote the similarity loss. The hard-constrained similarity loss is defined as the regularized objective:

$$\mathcal{L}_{\text{HCS}} = \lambda \mathcal{L}_{\text{cls}}(\theta) + (1 - \lambda) \mathcal{L}_{\text{CKA}}(\theta) \quad (7)$$

where $\lambda \in [0, 1]$ is a parameter that balances the task loss and the similarity loss. By default, $\lambda := 0.8$, and this value yields the best classification results and similarity.

$\mathcal{L}_{\text{cls}}(\theta)$ is the classification loss in Eq. 1, and $\mathcal{L}_{\text{CKA}}(\theta)$ quantifies the representation dissimilarity through:

$$\mathcal{L}_{\text{CKA}}(\theta) = 1 - CKA(\mathbf{F}_{\theta_0}, \mathbf{F}_\theta) \quad (8)$$

Orthogonal manifold-constrained reformulation. The original constrained optimization in Equation (6) requires computationally expensive similarity evaluations over full dataset representations. By exploiting the invariance properties of Centered Kernel Alignment (CKA), we reformulate the problem within a similarity-invariant manifold \mathcal{M} . The constrained optimization reduces to an unconstrained problem:

$$\theta^* = \arg \min_{\theta \in \mathcal{M}_{\theta_0}} \mathcal{L}(\theta) \quad (9)$$

This reparameterization implicitly preserves representation similarity through the manifold structure \mathcal{M} , eliminating explicit CKA computations during optimization while maintaining $CKA(\mathbf{F}_{\theta_0}, \mathbf{F}_\theta) \geq \epsilon$ by design.

3.3. Orthogonal Alignment of Statistical Measures

To address the challenge of nonlinear models with layer-wise activations, we propose a global orthogonal alignment mechanism using a learnable orthogonal matrix \mathbf{Q} and scaling factor α . The objective minimizes:

$$\mathbb{E}_{\mathbf{X} \sim \mathcal{D}} \|\mathbf{F}_\theta(\mathbf{X}) - \alpha \mathbf{F}_{\theta_0}(\mathbf{X}) \mathbf{Q}\|_F^2 \quad (10)$$

To achieve computational efficiency, we approximate this through statistical moment matching:

$$\|\boldsymbol{\mu}_\theta - \alpha \mathbf{Q} \boldsymbol{\mu}_{\theta_0}\|_F^2 \quad \text{and} \quad \|\boldsymbol{\Sigma}_\theta - \mathbf{Q}^\top \boldsymbol{\Sigma}_{\theta_0} \mathbf{Q}\|_F^2 \quad (11)$$

where $\boldsymbol{\mu}_\theta = \mathbb{E}_{\mathbf{X}}[\mathbf{F}_\theta(\mathbf{X})]$ and $\boldsymbol{\Sigma}_\theta = \text{Cov}(\mathbf{F}_\theta(\mathbf{X}), \mathbf{F}_\theta(\mathbf{X}))$ capture first- and second-order statistics.

Omission of α and $\boldsymbol{\mu}_\theta$. In Eq. 11, the combined effect of $\alpha \mathbf{Q}$ renders the constraint on $\boldsymbol{\mu}_\theta$ redundant. Consequently, as shown in Fig. 2, the objective is modified to:

$$\|\boldsymbol{\Sigma}_\theta - \mathbf{Q}^\top \boldsymbol{\Sigma}_{\theta_0} \mathbf{Q}\|_F^2 \quad (12)$$

Definition 5 (Orthogonal Manifold Similarity Loss: RepSim). *Let $\boldsymbol{\Sigma}_{\theta_0}$ and $\boldsymbol{\Sigma}_\theta$ denote the covariance of the output distribution parameterized by θ_0 and θ , respectively. Let \mathbf{Q} be a Orthogonal matrix that aligns the object in Eq. 12. The total loss, referred to as RepSim, is formally defined as*

$$\mathcal{L}_{\text{RepSim}}(\theta, \mathbf{Q}) = \mathcal{L}_{\text{cls}}(\theta) + \mathcal{L}_{\text{Cov}}(\theta, \mathbf{Q}) \quad (13)$$

where the regularization loss is given by

$$\mathcal{L}_{\text{Cov}}(\theta, \mathbf{Q}) = \|\boldsymbol{\Sigma}_\theta - \mathbf{Q}^\top \boldsymbol{\Sigma}_{\theta_0} \mathbf{Q}\|_F^2 \quad (14)$$

Loss in Eq. 13 enforces transferability on first-order moments while preserving structural invariance under orthogonal transformations for second-order moments. The orthonormal constraint $\mathbf{Q} \in \mathcal{V}_{d,d}$ ensures the isometric property in feature space rotations. Explicit decoupling of mean-covariance alignment reduces computational complexity to $O(d^2)$ through trace operations, while maintaining geometric consistency in the representation space. This reduction in complexity from $O(nd^2)$ to $O(d^2)$ preserves geometric structure through orthogonal covariance transformations.

4. Experiment

4.1. Setting

Our downstream task mainly focuses on the medical image classification. The baseline model is a Vision Transformer [9] (ViT-B/16) with 12 Transformer encoder layers, an embedding dimension of 768, and 12 attention heads per layer. The model is initialized with pretrained weights. Various finetuning strategies are compared: full finetuning (FULL) of all parameters, finetuning only the classification head (LINEAR), training from scratch (SCRATCH), hard similarity-constrained finetuning (HCS), and our RepSim. We also compare the most three structural relevant PEFT methods in compatibility evaluation, *e.g.*, Adaptformer, LoRA and Partial-3. Evaluation metrics include CKA (which measures the representation similarity between pretrained and finetuned models) as well as accuracy (Acc) and mean Average Precision (mAP) for assessing classification performance. For evaluation, we use five medical image classification datasets: ISIC2018 [7], APTOS2019 [21], and three datasets from MedFM dataset [41] (namely, MedFM-Chest, MedFM-Colon, and MedFM-Endo). These datasets cover various modalities, including skin lesions, diabetic retinopathy diagnosis, chest X-rays, pathology, and colonoscopy images, and they encompass multi-class, binary, and multi-label classification tasks, with comparable dataset sizes. Additional details on the training and evaluation settings are provided in the supplementary materials.

4.2. Main Result

4.2.1. Overall Result on Five Medical Datasets

Training from scratch and finetuning results. As shown in Tab. 1, training from scratch (SCRATCH) achieves the lowest classification accuracy and representation similarity, even lower than finetuning only the classification head (LINEAR), supporting that pretrained models provide a good initialization. Compared to FULL finetuning, finetuning only the classification head shows a clear limitation in classification ability, with a gap of 11.61, indicating that finetuning more parameters is necessary. However, the results from RepSim demonstrate that high accuracy does not necessarily require a drastic drop in similarity. RepSim achieves an average result across all datasets that is only 0.99 lower than FULL finetuning, while improving similarity by 0.16 (a greater than 30% improvement compared to 0.52). The anomalies in the results of MedFM-Chest and MedFM-Endo may stem from differences between upstream and downstream tasks, as the pretraining task is multi-class classification, while the fine-tuning task is multi-label classification. Notably, on the ISIC2018 dataset, accuracy drops by 0.68, but similarity increases by 0.28 (nearly a 90% improvement compared to 0.32). Furthermore, although hard-constrained methods show a higher increase in accuracy than RepSim,

Metric	Model	ISIC2018 Acc (n=10k)	APTOS2019 Acc (n=2.9k)	MedFM-Chest mAP (n=2.1k)	MedFM-Colon Acc (n=5.6k)	MedFM-Endo mAP (n=1.8k)	Avg.
Accuracy	FULL	84.63±0.08	84.06±0.42	33.56±1.29	99.74±0.30	58.11±2.54	72.02
	LINEAR	73.57±0.31	77.87±0.47	23.55±0.11	94.24±0.20	37.80±0.58	61.41
	SCRATCH	66.91±0.10	69.49±0.42	11.89±0.21	89.42±0.94	17.08±0.15	50.96
	HCS $\lambda(0.8)$	83.20±0.17	83.52±1.23	26.86±2.23	98.95±0.37	51.41±2.72	68.79 ($\downarrow 3.23$)
	RepSim (ours)	83.95±0.80	83.61±0.47	33.11±1.52	99.05±0.11	55.42±0.48	71.03 ($\downarrow 0.99$)
Similarity	FULL	0.32±0.01	0.52±0.01	0.58±0.03	0.58±0.07	0.61±0.00	0.52
	SCRATCH	0.36±0.01	0.37±0.03	0.47±0.02	0.67±0.02	0.39±0.00	0.45
	HCS $\lambda(0.8)$	0.75±0.07	0.77±0.07	0.62±0.03	0.90±0.04	0.77±0.02	0.76 ($\uparrow 0.24$)
	RepSim (ours)	0.60±0.02	0.73±0.03	0.55±0.04	0.82±0.02	0.70±0.02	0.68 ($\uparrow 0.16$)

Bold Highest accuracy or similarity (\uparrow) Improved similarity compared to FULL (\downarrow) Decrease in accuracy compared to FULL

Table 1. Image classification accuracy and similarity of finetuned models with or without pretrained model initialization. For each task, the average result from 3 runs is reported. *Similarity* denotes the CKA similarity (compared with pretrained model). HCS $\lambda(0.8)$ is the default hard-constrained method, due to its good balance between accuracy and similarity. Best results except FULL(accuracy) and HCS (similarity) are bolded.

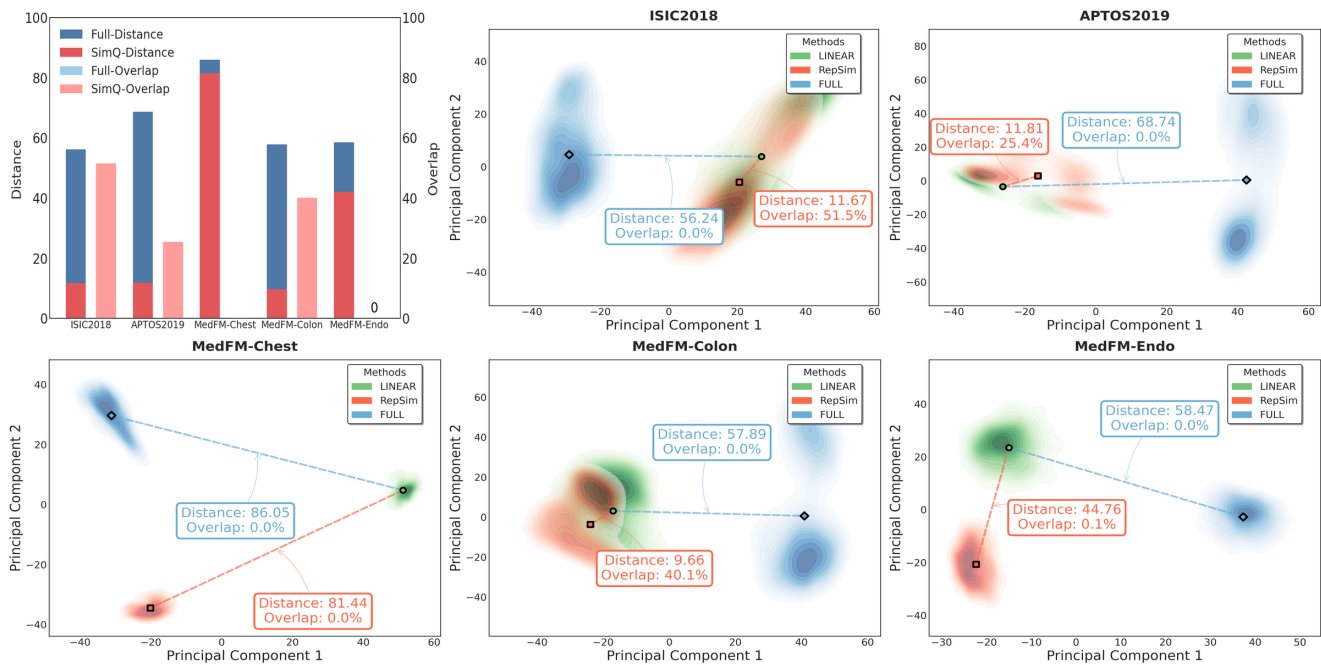


Figure 3. A comprehensive comparison of the PCA distribution results of pretrained model backbone (LINEAR), direct finetuning (FULL), and RepSim (ours) features on five corresponding medical datasets. The first figure summarizes the comparison of distance and overlap of pretrained backbone (LINEAR). Darker colors represent higher density of sample features, while lighter colors represent lower density.

they experience a more significant drop in accuracy. Overall, RepSim is a good alternative for the similarity-accuracy trade-off compared to the hard-constrained method (HCS).

RepSim method shares the representation of pretrained model. Fig. 3 shows the feature distribution results of samples extracted from pretrained and finetuned models. The bar

charts summarize the distance from the pretrained model’s feature center to the finetuned model’s feature center, as well as the overlap between features. The direct finetuning (FULL) method shows a noticeable distance and lack of overlap between features, indicating significant representation differences compared to the pretrained model features (LINEAR). In contrast, the RepSim method exhibits a high

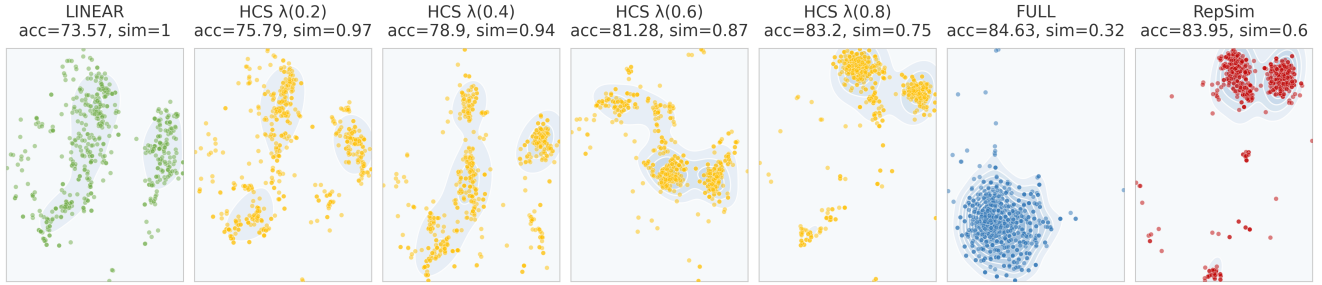


Figure 4. The t-SNE distribution visualization for a specific category sample from ISIC2018. The pretrained model backbone (LINEAR) exhibits a significant gap in the feature distribution of samples from this category. Direct finetuning eliminates this gap. However, preserving the representation similarity during finetuning helps retain this characteristic. Darker colors represent higher density of sample features, while lighter colors represent lower density.

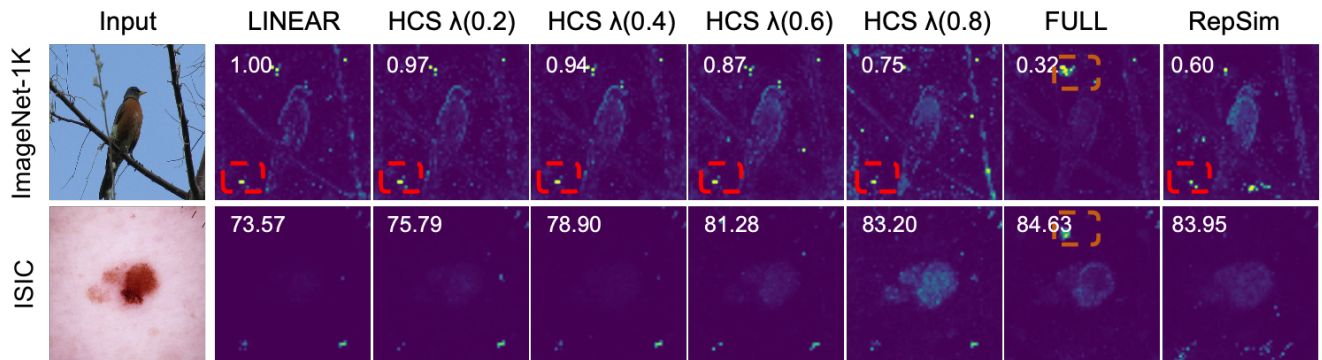


Figure 5. Visualization of attention maps for different finetuning methods. The first row shows the degree to which the finetuned model retains original knowledge. The second row shows the degree to which the finetuned model learns new knowledge.

overlap of pretrained features on the ISIC2018, APTOS2019, and MedFM-Colon datasets. Even for the multi-label classification datasets, MedFM-Chest and MedFM-Endo, although the expected overlap is not observed, the distance is closer compared to the FULL method. These results demonstrate the effectiveness of the RepSim method in preserving pretrained model features and support the hypothesis that the model shares the same representation [17].

4.2.2. Similarity Analysis on ISIC2018 Dataset

To further refine the representation similarity after finetuning, we focus on the experiments conducted on the ISIC2018 dataset. Given that ISIC2018 exhibited relatively low similarity under FULL finetuning in the previously presented results, and considering that it is a multi-class dataset with moderate scale and task difficulty, it serves as an ideal candidate for detailed analysis.

RepSim can preserve the pretrained model representation while adapting to downstream task representations.

Fig. 4 shows the t-SNE visualization of sample features for a target class (Benign Keratosis-like Lesions) from the ISIC2018 dataset. For this target class, the representation of

the pretrained model backbone (LINEAR) exhibits a clear gap, which is unusual for samples from the same class. The classification results also confirm the limitation of this representation in terms of classification. However, to improve classification accuracy, as the similarity constraint is reduced, with λ from 0.2 to 0.8, the representation becomes progressively closer to the fully finetuned representation, with the gap gradually disappearing and the features clustering in a single region. Our RepSim method effectively captures this balance, with most samples clustering into a tighter region while maintaining two distinct density centers.

Visualization of attention maps demonstrating learning and forgetting.

As shown in Fig. 5, the first row illustrates the changes in the attention maps of the pretrained model as similarity decreases. After finetuning directly on the ISIC2018 dataset (FULL), the attention to the ImageNet-1K image target (bird) vanishes. In contrast, applying a direct similarity constraint (HCS) or an indirect constraint (RepSim) preserves attention to the target object, even retaining artifacts (red dashed box). The second row shows that as classification accuracy improves, the finetuned model gradually enhances its attention to the target object (skin lesion).

Metric	Model	ISIC2018	APTOS2019	MedFM-Chest	MedFM-Colon	MedFM-Endo	Avg.
$\max_{\ \epsilon\ \leq \rho} \mathcal{L}_{\text{cls}}(\theta + \epsilon) \downarrow$	LINEAR	0.7292	0.6442	4.7553	0.1995	1.1375	1.4931
	FULL	0.6398	0.5701	4.3836	0.0509	1.0859	1.3461
	RepSim (ours)	0.5558	0.5262	4.3338	0.0677	1.0036	1.2974
$\mathcal{L}_{\text{cls}}(\theta) \downarrow$	LINEAR	0.7159	0.5989	4.7415	0.1841	1.1343	1.4749
	FULL	0.6125	0.5049	4.3727	0.0305	1.0743	1.3190
	RepSim (ours)	0.5312	0.5082	4.3236	0.0496	0.9957	1.2817
Sharpness \downarrow	LINEAR	0.0133	0.0453	0.0138	0.0154	0.0032	0.0182
	FULL	0.0273	0.0652	0.0109	0.0204	0.0116	0.0271
	RepSim (ours)	0.0246	0.0180	0.0102	0.0181	0.0080	0.0158

Table 2. Comparison of the generalizability, validated by sharpness $\max_{\|\epsilon\| \leq \rho} \mathcal{L}_{\text{cls}}(\theta + \epsilon) - \mathcal{L}_{\text{cls}}(\theta)$ with lower values indicating better generalization, across methods: FULL, RepSim (ours), and LINEAR (pretrained model backbone), with $\rho = 0.01$. Best results are bolded.

Notably, the artifacts from the pretrained model are also preserved. For FULL finetuning, the artifacts (orange dashed box) appear in both ImageNet-1K and ISIC2018 images. These observations highlight the necessity of considering similarity constraints.

4.3. Why Preserve Representation Similarity

RepSim achieves flatter minima. Generalizability is one of the most critical evaluation criteria and is considered a typical advantage of pretrained models, as they provide a good initialization. This section evaluates the generalizability of finetuned models by comparing sharpness, measured through the difference $\max_{\|\epsilon\| \leq \rho} \mathcal{L}_{\text{cls}}(\theta + \epsilon) - \mathcal{L}_{\text{cls}}(\theta)$, across finetuning methods. Lower sharpness reflects better generalizability. The results in Tab. 2 compare the generalizability of full finetuning (FULL), RepSim (our method), and the pretrained model backbone (LINEAR). The LINEAR method outperforms FULL with an average sharpness of 0.0182, demonstrating its robustness due to the pretrained initialization. FULL exhibits a higher average sharpness of 0.0271, indicating weaker generalization. RepSim achieves the lowest average sharpness of 0.0158, demonstrating its ability to achieve flatter minima and better generalization. Notably, RepSim consistently performs better than FULL across all datasets, with particularly strong results on APTOS2019, where its sharpness (0.0180) is significantly lower than that of FULL (0.0652). These results highlight RepSim’s effectiveness in bridging the gap between pretrained models and finetuned models, offering a promising approach for improving generalization in model optimization.

Enhanced parameter centrality for multi-task learning.

Results in Tab. 3 demonstrate that the RepSim method exhibits better parameter centrality across multiple datasets, thereby validating its adaptability in multi-task training. Specifically, the RepSim method significantly reduces the distance of model parameters to the average parameter center on four datasets: ISIC2018, APTOS2019, MedFM-Chest,

Dataset	FULL	RepSim	Change \downarrow
ISIC2018	1.35	0.93	$\downarrow 0.42$
APTOS2019	0.49	0.45	$\downarrow 0.04$
MedFM-Chest	1.02	0.98	$\downarrow 0.04$
MedFM-Colon	0.45	0.67	$\uparrow 0.22$
MedFM-Endo	0.68	0.58	$\downarrow 0.10$
Avg.	0.80	0.72	$\downarrow 0.08$

Table 3. Comparison of parameter distance to average center for FULL and RepSim methods across five datasets.

Method	FULL		RepSim	
	Acc	Sim	Acc	Sim
LoRA [16] (r=4)	73.34	0.847	73.74 \uparrow	0.865 \uparrow
Adaptformer [5] (r=64)	79.83	0.517	77.56 \downarrow	0.742 \uparrow
Partial-3 [19]	77.27	0.844	76.48 \downarrow	0.964 \uparrow

Table 4. Comparative analysis of RepSim on parameter-efficient finetuning methods.

and MedFM-Endo, with reductions of 0.42, 0.04, 0.04, and 0.10, respectively. Although the distance increases slightly (by 0.22) on the MedFM-Colon dataset, the overall performance of RepSim remains superior to the FULL method, with an average distance reduction of 0.08. These results indicate that the RepSim method can more effectively extract shared features, achieving better parameter centrality and generalization in multi-task training.

Apply RepSim to parameter-efficient finetuning. Tab. 4 demonstrates the compatibility of our method with parameter-efficient finetuning (PEFT) techniques, showcasing distinct research objectives and effects while enabling their integration. The results indicate that RepSim can be

Matrix Q	Accuracy	Similarity	mean μ	Accuracy	Similarity	Batch Size	Accuracy	Similarity
Fixed Q	83.55	0.56	w/ μ	83.49	0.51	4	81.42	0.21
Learnable Q	83.95 \uparrow	0.60 \uparrow	w/o μ	83.95 \uparrow	0.60 \uparrow	32	83.33	0.30
						128	83.95 \uparrow	0.60 \uparrow

(a) Ablation of matrix Q. (b) Ablation of aligning μ . (c) Ablation of batch size.

Table 5. Ablation results of fixed Q, aligning μ , and batch size.

effectively combined with various PEFT methods, such as LoRA, Adaptformer, and Partial-3, without significant performance degradation. Specifically, LoRA achieves a marginal improvement in both accuracy (73.34 to 73.74) and similarity (0.847 to 0.865) when RepSim is applied. For Adaptformer, while accuracy slightly decreases from 79.83 to 77.56, similarity significantly improves from 0.517 to 0.742, highlighting RepSim’s ability to enhance feature alignment. Partial-3 exhibits a trade-off, with a minor accuracy drop from 77.27 to 76.48 but a substantial similarity increase from 0.844 to 0.964, further emphasizing the complementary nature of RepSim and PEFT. These findings underscore that RepSim and PEFT are not mutually exclusive but can be synergistically combined to achieve balanced performance in accuracy and feature similarity.

Metric	LINEAR	FULL	HCS	RepSim
One Iteration (s)	3.91	8.38	16.68	8.47
50 Epochs (min)	26.65	57.08	111.04	57.83

Table 6. Training time per iteration and for 50 epochs on single NVIDIA A100 40G with a batch size of 128.

Training time comparison. The results in Tab. 6 reveal significant variations in training efficiency across the evaluated methods. The LINEAR method demonstrates the fastest performance, requiring the least time for both per-iteration and full-epoch training. In contrast, the FULL and RepSim methods exhibit nearly identical computational costs, suggesting comparable efficiency. Notably, the HCS method incurs the highest computational overhead, making it the least efficient among the tested approaches.

4.4. Ablation Study

Ablation studies are conducted to further explore the impact of different components. The key differences among the examined methods lie in whether the Q matrix is learnable, the application of mean alignment (using μ), and the chosen batch size.

Ablation of matrix Q. As shown in Tab. 5 (a), employing a learnable Q matrix improves accuracy and similarity metrics by 0.4% and 0.04, respectively, compared to using

a fixed Q parameter. This demonstrates that a learnable orthogonal matrix can more effectively capture features.

Ablation of alignment of μ . Tab. 5 (b) further reveals that the absence of mean alignment (w/o μ) yields superior performance in both accuracy and similarity metrics, with improvements of 0.46% and 0.09, respectively, compared to the case where mean alignment is applied (w/ μ). This suggests that the mean alignment operation may introduce unnecessary constraints on the feature distribution, thereby hindering the model’s ability to fully exploit the underlying data structure. Removing this alignment allows the model to learn more flexible representations, leading to enhanced performance.

Ablation of batch size. Increasing the batch size from 4 to 128, as shown in Tab. 5 (c), significantly boosts accuracy and similarity metrics, with improvements of 2.53% and 0.39, respectively. A larger batch size provides a more accurate estimation of the covariance matrix. The observed trend underscores the importance of selecting an appropriate batch size.

5. Conclusion

This paper provides a new insight on finetuning, *i.e.*, keeping representation similarity. Inspired by the Occam’s Razor and low-dimensionality dynamics in many biological systems, we propose a new finetuning method RepSim based on the representation similarity, which minimizes the distance between pretrained representations and finetuned representations via constraining learnable orthogonal manifold based on similarity invariance. Experiments show that RepSim maintains competitive performance while significantly improving representation similarity and generalizability, indicating that pretrained representations can be preserved well while still effectively adapting to downstream tasks. It also achieves superior performance and efficiency to the hard regularization, compatibility with other finetuning methods, *e.g.*, PEFT, and potential in multi-task learning. In the future, RepSim can be extended to more models, datasets and tasks. To better preserve pretrained foundation model’s original abilities, more physical or biological-inspired constraints may be introduced to further reduce the system’s freedom degree. As the reasoning model arises, it is also interesting to explore whether the chain of thought of pretrained models

can be preserved through similarity-based approaches during finetuning.

References

- [1] Mmclassification. <https://github.com/openmmlab/mclassification>. 11
- [2] Muhammad Awais, Muzammal Naseer, Salman Khan, Rao Muhammad Anwer, Hisham Cholakkal, Mubarak Shah, Ming-Hsuan Yang, and Fahad Shahbaz Khan. Foundation models defining a new era in vision: a survey and outlook. *IEEE Transactions on Pattern Analysis and Machine Intelligence*, 2025. 1
- [3] Hyojin Bahng, Ali Jahanian, Swami Sankaranarayanan, and Phillip Isola. Exploring visual prompts for adapting large-scale models. *arXiv preprint arXiv:2203.17274*, 2022. 2
- [4] Rishi Bommasani, Drew A Hudson, Ehsan Adeli, Russ Altman, Simran Arora, Sydney von Arx, Michael S Bernstein, Jeannette Bohg, Antoine Bosselut, Emma Brunskill, et al. On the opportunities and risks of foundation models. *arXiv preprint arXiv:2108.07258*, 2021. 1
- [5] Shoufa Chen, Chongjian Ge, Zhan Tong, Jiangliu Wang, Yibing Song, Jue Wang, and Ping Luo. Adaptformer: Adapting vision transformers for scalable visual recognition. *Advances in Neural Information Processing Systems*, 35:16664–16678, 2022. 1, 2, 7
- [6] Wei Chen, Zichen Miao, and Qiang Qiu. Inner product-based neural network similarity. *Advances in Neural Information Processing Systems*, 36:73995–74020, 2023. 2
- [7] Noel Codella, Veronica Rotemberg, Philipp Tschandl, M Emre Celebi, Stephen Dusza, David Gutman, Brian Helba, Aadi Kaloo, Konstantinos Liopyris, Michael Marchetti, et al. Skin lesion analysis toward melanoma detection 2018: A challenge hosted by the international skin imaging collaboration (isic). *arXiv preprint arXiv:1902.03368*, 2019. 4, 11
- [8] Ning Ding, Yujia Qin, Guang Yang, Fuchao Wei, Zonghan Yang, Yusheng Su, Shengding Hu, Yulin Chen, Chi-Min Chan, Weize Chen, et al. Parameter-efficient fine-tuning of large-scale pre-trained language models. *Nature Machine Intelligence*, 5(3):220–235, 2023. 2
- [9] Alexey Dosovitskiy, Lucas Beyer, Alexander Kolesnikov, Dirk Weissenborn, Xiaohua Zhai, Thomas Unterthiner, Mostafa Dehghani, Matthias Minderer, Georg Heigold, Sylvain Gelly, et al. An image is worth 16x16 words: Transformers for image recognition at scale. *arXiv preprint arXiv:2010.11929*, 2020. 4, 11
- [10] Alaaeldin El-Nouby, Michal Klein, Shuangfei Zhai, Miguel Ángel Bautista, Vaishaal Shankar, Alexander T Tsochev, Joshua M Susskind, and Armand Joulin. Scalable pre-training of large autoregressive image models. In *International Conference on Machine Learning*, pages 12371–12384. PMLR, 2024. 2
- [11] Tetsuhiro S Hatakeyama and Kunihiko Kaneko. Reciprocity between robustness of period and plasticity of phase in biological clocks. *Physical Review Letters*, 115(21):218101, 2015. 2
- [12] Soufiane Hayou, Nikhil Ghosh, and Bin Yu. Lora+: Efficient low rank adaptation of large models. In *International Conference on Machine Learning*, pages 17783–17806. PMLR, 2024. 2
- [13] Kaiming He, Xinlei Chen, Saining Xie, Yanghao Li, Piotr Dollár, and Ross Girshick. Masked autoencoders are scalable vision learners. In *Proceedings of the IEEE/CVF conference on computer vision and pattern recognition*, pages 16000–16009, 2022. 2
- [14] Ruidan He, Linlin Liu, Hai Ye, Qingyu Tan, Bosheng Ding, Liying Cheng, Jiawei Low, Lidong Bing, and Luo Si. On the effectiveness of adapter-based tuning for pretrained language model adaptation. In *Proceedings of the 59th Annual Meeting of the Association for Computational Linguistics and the 11th International Joint Conference on Natural Language Processing (Volume 1: Long Papers)*, pages 2208–2222, 2021. 2
- [15] Ruifei He, Shuyang Sun, Jihan Yang, Song Bai, and Xiaojuan Qi. Knowledge distillation as efficient pre-training: Faster convergence, higher data-efficiency, and better transferability. In *Proceedings of the IEEE/CVF conference on computer vision and pattern recognition*, pages 9161–9171, 2022. 2
- [16] Edward J Hu, Yelong Shen, Phillip Wallis, Zeyuan Allen-Zhu, Yuanzhi Li, Shean Wang, Lu Wang, Weizhu Chen, et al. Lora: Low-rank adaptation of large language models. *ICLR*, 1(2):3, 2022. 1, 2, 7
- [17] Minyoung Huh, Brian Cheung, Tongzhou Wang, and Phillip Isola. Position: The platonic representation hypothesis. In *Forty-first International Conference on Machine Learning*, 2024. 1, 6
- [18] Joana Palés Huix, Adithya Raju Ganeshan, Johan Fredin Haslum, Magnus Söderberg, Christos Matsoukas, and Kevin Smith. Are natural domain foundation models useful for medical image classification? In *Proceedings of the IEEE/CVF winter conference on applications of computer vision*, pages 7634–7643, 2024. 1
- [19] Menglin Jia, Luming Tang, Bor-Chun Chen, Claire Cardie, Serge Belongie, Bharath Hariharan, and Ser-Nam Lim. Visual prompt tuning. In *European Conference on Computer Vision*, pages 709–727. Springer, 2022. 1, 2, 7
- [20] Jared Kaplan, Sam McCandlish, Tom Henighan, Tom B Brown, Benjamin Chess, Rewon Child, Scott Gray, Alec Radford, Jeffrey Wu, and Dario Amodei. Scaling laws for neural language models. *arXiv preprint arXiv:2001.08361*, 2020. 2
- [21] Maggie Karthik and Sohier Dane. Aptos 2019 blindness detection (2019). URL <https://kaggle.com/competitions/aptos2019-blindness-detection>. 4, 11
- [22] Alexander Kirillov, Eric Mintun, Nikhila Ravi, Hanzi Mao, Chloe Rolland, Laura Gustafson, Tete Xiao, Spencer Whitehead, Alexander C Berg, Wan-Yen Lo, et al. Segment anything. In *Proceedings of the IEEE/CVF international conference on computer vision*, pages 4015–4026, 2023. 2
- [23] Simon Kornblith, Mohammad Norouzi, Honglak Lee, and Geoffrey Hinton. Similarity of neural network representations revisited. In *International conference on machine learning*, pages 3519–3529. PMLR, 2019. 2, 3
- [24] Ananya Kumar, Aditi Raghunathan, Robbie Jones, Tengyu Ma, and Percy Liang. Fine-tuning can distort pretrained features and underperform out-of-distribution. In *International Conference on Learning Representations*, 2022. 1

- [25] Yiming Liang, Tianyu Zheng, Xinrun Du, Ge Zhang, Jiaheng Liu, Xingwei Qu, Wenqiang Zu, Xingrun Xing, Chujie Zheng, Lei Ma, et al. Aligning instruction tuning with pre-training. *arXiv preprint arXiv:2501.09368*, 2025. 2
- [26] Haotian Liu, Chunyuan Li, Qingyang Wu, and Yong Jae Lee. Visual instruction tuning. *Advances in neural information processing systems*, 36:34892–34916, 2023. 2
- [27] Shih-Yang Liu, Chien-Yi Wang, Hongxu Yin, Pavlo Molchanov, Yu-Chiang Frank Wang, Kwang-Ting Cheng, and Min-Hung Chen. Dora: Weight-decomposed low-rank adaptation. In *Forty-first International Conference on Machine Learning*, 2024. 2
- [28] Weiyang Liu, Rongmei Lin, Zhen Liu, Lixin Liu, Zhiding Yu, Bo Dai, and Le Song. Learning towards minimum hyperspherical energy. *Advances in neural information processing systems*, 31, 2018. 1
- [29] Weiyang Liu, Rongmei Lin, Zhen Liu, Lixin Liu, Zhiding Yu, Bo Dai, and Le Song. Learning towards minimum hyperspherical energy. *Advances in neural information processing systems*, 31, 2018. 2
- [30] Weiyang Liu, Zeju Qiu, Yao Feng, Yuliang Xiu, Yuxuan Xue, Longhui Yu, Haiwen Feng, Zhen Liu, Juyeon Heo, Songyou Peng, et al. Parameter-efficient orthogonal finetuning via butterfly factorization. In *ICLR*, 2024. 1, 2
- [31] Kai Lv, Yuqing Yang, Tengxiao Liu, Qipeng Guo, and Xipeng Qiu. Full parameter fine-tuning for large language models with limited resources. In *Proceedings of the 62nd Annual Meeting of the Association for Computational Linguistics (Volume 1: Long Papers)*, pages 8187–8198, 2024. 1, 2
- [32] Ari Morcos, Maithra Raghu, and Samy Bengio. Insights on representational similarity in neural networks with canonical correlation. *Advances in neural information processing systems*, 31, 2018. 3
- [33] Maxat Nurgazin and Nguyen Anh Tu. A comparative study of vision transformer encoders and few-shot learning for medical image classification. In *Proceedings of the IEEE/CVF International Conference on Computer Vision*, pages 2513–2521, 2023. 1
- [34] Maxime Oquab, Timothée Darcet, Théo Moutakanni, Huy Vo, Marc Szafraniec, Vasil Khalidov, Pierre Fernandez, Daniel Haziza, Francisco Massa, Alaaeldin El-Nouby, et al. Dinov2: Learning robust visual features without supervision. *Transactions on Machine Learning Research Journal*, pages 1–31, 2024. 2
- [35] Zeju Qiu, Weiyang Liu, Haiwen Feng, Yuxuan Xue, Yao Feng, Zhen Liu, Dan Zhang, Adrian Weller, and Bernhard Schölkopf. Controlling text-to-image diffusion by orthogonal finetuning. *Advances in Neural Information Processing Systems*, 36:79320–79362, 2023. 1, 2
- [36] Alec Radford, Jong Wook Kim, Chris Hallacy, Aditya Ramesh, Gabriel Goh, Sandhini Agarwal, Girish Sastry, Amanda Askell, Pamela Mishkin, Jack Clark, et al. Learning transferable visual models from natural language supervision. In *International conference on machine learning*, pages 8748–8763. PmLR, 2021. 2
- [37] Zhiqiang Shen, Zechun Liu, Jie Qin, Marios Savvides, and Kwang-Ting Cheng. Partial is better than all: Revisiting finetuning strategy for few-shot learning. In *Proceedings of the AAAI conference on artificial intelligence*, pages 9594–9602, 2021. 2
- [38] Yi-Lin Sung, Jaemin Cho, and Mohit Bansal. VI-adapter: Parameter-efficient transfer learning for vision-and-language tasks. In *Proceedings of the IEEE/CVF conference on computer vision and pattern recognition*, pages 5227–5237, 2022. 2
- [39] Qian-Yuan Tang, Tetsuhiro S Hatakeyama, and Kunihiko Kaneko. Functional sensitivity and mutational robustness of proteins. *Physical Review Research*, 2(3):033452, 2020. 2
- [40] Hugo Touvron, Thibaut Lavril, Gautier Izacard, Xavier Martinet, Marie-Anne Lachaux, Timothée Lacroix, Baptiste Rozière, Naman Goyal, Eric Hambro, Faisal Azhar, et al. Llama: Open and efficient foundation language models. *arXiv preprint arXiv:2302.13971*, 2023. 2
- [41] Dequan Wang, Xiaosong Wang, Lilong Wang, Mengzhang Li, Qian Da, Xiaoqiang Liu, Xiangyu Gao, Jun Shen, Junjun He, Tian Shen, et al. A real-world dataset and benchmark for foundation model adaptation in medical image classification. *Scientific Data*, 10(1):574, 2023. 1, 4, 11
- [42] Liyuan Wang, Xingxing Zhang, Hang Su, and Jun Zhu. A comprehensive survey of continual learning: Theory, method and application. *IEEE Transactions on Pattern Analysis and Machine Intelligence*, 2024. 1
- [43] Chenwei Wu, Holden Lee, and Rong Ge. Connecting pre-trained language model and downstream task via properties of representation. *Advances in Neural Information Processing Systems*, 36:47216–47238, 2023. 2
- [44] Yi Xin, Junlong Du, Qiang Wang, Ke Yan, and Shouhong Ding. Mmap: Multi-modal alignment prompt for cross-domain multi-task learning. In *Proceedings of the AAAI Conference on Artificial Intelligence*, pages 16076–16084, 2024. 1
- [45] Sihyun Yu, Sangkyung Kwak, Huiwon Jang, Jongheon Jeong, Jonathan Huang, Jinwoo Shin, and Saining Xie. Representation alignment for generation: Training diffusion transformers is easier than you think. In *The Thirteenth International Conference on Learning Representations*, 2025. 2
- [46] Lu Yuan, Dongdong Chen, Yi-Ling Chen, Noel Codella, Xiyang Dai, Jianfeng Gao, Houdong Hu, Xuedong Huang, Boxin Li, Chunyuan Li, et al. Florence: A new foundation model for computer vision. *arXiv preprint arXiv:2111.11432*, 2021. 1
- [47] Lvmin Zhang, Anyi Rao, and Maneesh Agrawala. Adding conditional control to text-to-image diffusion models. In *Proceedings of the IEEE/CVF international conference on computer vision*, pages 3836–3847, 2023. 2
- [48] Shaoting Zhang and Dimitris Metaxas. On the challenges and perspectives of foundation models for medical image analysis. *Medical image analysis*, 91:102996, 2024. 1
- [49] Yu Zhang and Qiang Yang. A survey on multi-task learning. *IEEE transactions on knowledge and data engineering*, 34(12):5586–5609, 2021. 1
- [50] Wenqiang Zu, Shenghao Xie, Qing Zhao, Guoqi Li, and Lei Ma. Embedded prompt tuning: Towards enhanced calibration of pretrained models for medical images. *Medical Image Analysis*, 97:103258, 2024. 1, 2

Keeping Representation Similarity in Finetuning for Medical Image Analysis

Supplementary Material

A. Experiment Settings

We use the ViT-B/16 model [9], with an input image size of 224×224 and a patch size of 16. The pretrained model is trained in a supervised manner on ImageNet-1K. In our experiments, the batch size is set to 128 to obtain a better estimation of the covariance matrix of the fine-tuned features, and the learning rate is set to 6×10^{-4} . The experiments were conducted on 4 NVIDIA A100 40G GPUs, with each training session running for 50 epochs. Our code is built upon the MMClassification framework [1]. Tab. 7 presents detailed information about the experimental dataset.

Dataset	Modality	Task Type	Classes	Train	Test	Metric
ISIC2018 [7]	Dermoscopy	Multiclass	7	10,015	1,512	Accuracy
APTOS2019 [21]	Fundus	Multiclass	5	2,930	366	Accuracy
MedFM-Chest [41]	X-ray	Multi-label	19	2,140	3,869	mAP
MedFM-Colon [41]	Pathology	Binary	2	5,654	7,651	Accuracy
MedFM-Endo [41]	Endoscopy	Multi-label	4	1,810	2,936	mAP

Table 7. Details of the dataset specifications.

B. More Results

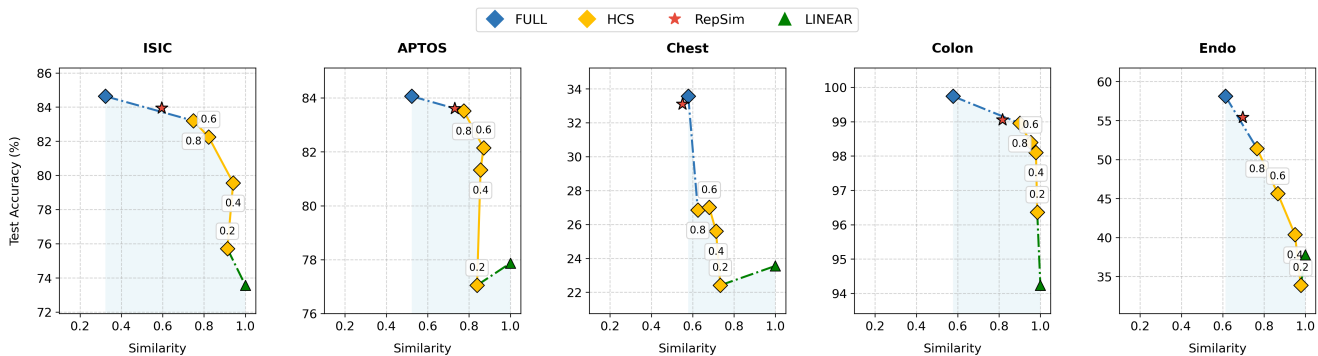


Figure 6. Similarity-accuracy curves of the hard-constrained similarity (HCS) method across different datasets. Models above the curve achieve a better balance between similarity preservation and accuracy. The λ values range from 0.8 to 0.2, indicating a gradual decrease in similarity loss weight.

Similarity and accuracy curve. As shown in Fig. 6, our proposed RepSim method consistently demonstrates an effective balance between similarity (sim) and accuracy (acc) across multiple datasets. Direct finetuning, the hard-constrained HCS method (λ ranges from 0.8 to 0.2), and finetuning only the linear classification head form the trade-off curve between classification accuracy and representation similarity (with pretrained model). Models above the curve indicate a better balance between accuracy and similarity, while those below the curve show the opposite. Direct finetuning achieves the highest classification accuracy but the lowest representation similarity. Additionally, the trade-off curve highlights the rapid decline in accuracy as similarity increases (with higher weight on HCS). Our proposed RepSim method shows comparable results on the ISIC2018, APTOS2019, MedFM-Colon, and MedFM-Endo datasets compared to the hard-constrained HCS. Although on the MedFM-Chest dataset, we failed to find a balance in the similarity-accuracy trade-off, these overall results strongly demonstrate that RepSim effectively leverages the trade-off between similarity and accuracy, avoiding the severe similarity degradation observed in the direct finetuning method (FULL) when enforcing high accuracy, thereby achieving superior overall performance.

C. Similarity Analysis

Assumption 6 (Parameter Space and Mapping Structure). *Let $\Theta \subseteq \mathbb{R}^m$ be a path-connected space, and $f_\theta : \mathcal{X} \rightarrow \mathbb{R}^d$ be continuous in θ . The constrained optimum θ_{cka} lies in similarity-invariant subsapce \mathcal{M}_{θ_0} with $\mathcal{L}(\theta_{cka}) = \min_{\theta \in \mathcal{M}_{\theta_0}} \mathcal{L}(\theta)$, while the unconstrained optimum $\theta_{loss} = \arg \min_{\theta \in \Theta} \mathcal{L}(\theta)$ satisfies $\theta_{loss} \notin \mathcal{M}_{\theta_0}$.*

Assumption 7 (Continuity). *The loss function $\mathcal{L}(\theta)$ and the similarity metric $CKA(\mathbf{F}_{\theta_0}, \mathbf{F}_\theta)$ are continuous over the parameter space Θ . Here, θ_0 and θ denote the parameters of the pre-trained model and the fine-tuned model, respectively.*

Proposition 8 (Existence of Intermediates). *Under the above assumptions 6 and 7, there exists a continuous path $\gamma : [0, 1] \rightarrow \Theta$ connecting θ_{cka} and θ_{loss} such that for any $t \in (0, 1)$, the intermediate parameter $\theta(t) = \gamma(t)$ satisfies:*

$$\begin{aligned} \mathcal{L}(\theta(t)) &\in (\mathcal{L}(\theta_{loss}), \mathcal{L}(\theta_{cka})) \\ CKA(f_{\theta(t)}, f_{\theta_0}) &\in (CKA(f_{\theta_{loss}}, f_{\theta_0}), 1) \end{aligned}$$

This establishes the inherent trade-off between representation similarity and task performance under minimal topological and continuity constraints.

Proof. Since Θ is path-connected and both θ_{cka} and θ_{loss} belong to Θ , there exists a continuous mapping $\gamma : [0, 1] \rightarrow \Theta$ satisfying $\gamma(0) = \theta_{cka}$ and $\gamma(1) = \theta_{loss}$.

Define the composite function

$$L(t) = \mathcal{L}(\gamma(t)) \tag{15}$$

The continuity of both γ and \mathcal{L} guarantees that $L(t)$ is continuous on $[0, 1]$, with

$$L(0) = \mathcal{L}(\theta_{cka}) \quad \text{and} \quad L(1) = \mathcal{L}(\theta_{loss}) \tag{16}$$

Since $\mathcal{L}(\theta_{loss}) < \mathcal{L}(\theta_{cka})$, the intermediate value theorem implies that for any value c satisfying

$$\mathcal{L}(\theta_{loss}) < c < \mathcal{L}(\theta_{cka}) \tag{17}$$

there exists some $t_c \in (0, 1)$ such that $L(t_c) = c$. Hence, every intermediate point $\gamma(t)$ along the path fulfills

$$\mathcal{L}(\theta_{loss}) < \mathcal{L}(\gamma(t)) < \mathcal{L}(\theta_{cka}) \tag{18}$$

Similarly, define

$$S(t) = CKA(f_{\gamma(t)}, f_{\theta_0}) \tag{19}$$

The continuity of γ and the CKA function ensures that $S(t)$ is continuous on $[0, 1]$, with

$$S(0) = CKA(f_{\theta_{cka}}, f_{\theta_0}) = 1 \quad \text{and} \quad S(1) = CKA(f_{\theta_{loss}}, f_{\theta_0}) < 1 \tag{20}$$

An application of the intermediate value theorem shows that for any s satisfying

$$CKA(f_{\theta_{loss}}, f_{\theta_0}) < s < 1 \tag{21}$$

there exists some $t_s \in (0, 1)$ such that $S(t_s) = s$. Therefore, every intermediate point satisfies

$$CKA(f_{\theta_{loss}}, f_{\theta_0}) < CKA(f_{\gamma(t)}, f_{\theta_0}) < 1 \tag{22}$$

It remains to demonstrate that there is at least one $t \in (0, 1)$ for which both intermediate conditions hold simultaneously. To this end, consider the sets

$$A = \{t \in [0, 1] \mid \mathcal{L}(\gamma(t)) < \mathcal{L}(\theta_{cka})\} \tag{23}$$

and

$$B = \{t \in [0, 1] \mid CKA(f_{\gamma(t)}, f_{\theta_0}) > CKA(f_{\theta_{loss}}, f_{\theta_0})\} \tag{24}$$

Since $L(1) = \mathcal{L}(\theta_{loss}) < \mathcal{L}(\theta_{cka})$, we have $1 \in A$, and since $S(0) = 1 > CKA(f_{\theta_{loss}}, f_{\theta_0})$, we have $0 \in B$. The continuity of $L(t)$ and $S(t)$ implies that both A and B are open subsets of $[0, 1]$. A short analysis shows that the intersection $A \cap B$ is nonempty. Thus, there exists some $t \in (0, 1)$ for which

$$\mathcal{L}(\theta_{loss}) < \mathcal{L}(\gamma(t)) < \mathcal{L}(\theta_{cka}) \tag{25}$$

and

$$CKA(f_{\theta_{loss}}, f_{\theta_0}) < CKA(f_{\gamma(t)}, f_{\theta_0}) < 1 \tag{26}$$

This completes the proof. \square